Nanoimprint pattern transfer quality from specular x-ray reflectivity

Hae-Jeong Lee, Christopher L. Soles,[a] Hyun Wook Ro, Ronald L. Jones, Eric K. Lin, and Wen-li Wu
Polymers Division, National Institute of Standards and Technology, 100 Bureau Drive, Gaithersburg, Maryland 20899-8541

Daniel R. Hines
Laboratory for Physical Sciences, University of Maryland, 8050 Greenmead Drive, College Park, Maryland 20740

(Received 11 April 2005; accepted 3 November 2005; published online 27 December 2005)

Specular x-ray reflectivity is used for high precision measurements of the pattern height, residual layer thickness, and the line-to-space ratio for parallel line and space patterns fabricated with nanoimprint lithography. The line-to-space ratio is profiled vertically to reveal relative linewidth variations as a function of the feature height. These relative linewidth variations are quantified through an external measure of the average pitch to fully define the line shape profile or cross section. An excellent fidelity of the nanoimprint pattern transfer process is quantified by comparing the line shape profiles of the mold to the imprinted pattern. © *2005 American Institute of Physics*. [DOI: 10.1063/1.2158512]

Nanoimprint lithography[1] (NIL) offers great potential as a high-resolution and economically viable next generation lithography for nanoscale patterning and nanofabrication. It has been recently shown that features as small as 5 nm can be fabricated with NIL,[2] but at these length scales it is difficult to *quantify* the quality of the nanoimprint process. Accurate pattern height and width measurements are critical to assess the fidelity of pattern transfer from the mold to the imprint. Equally as critical is the residual layer thickness of resist between the imprinted pattern and the supporting substrate.[3–5] Cross-sectional electron microscopy can provide high precision data, but calibration is often difficult and requires destruction of the sample. Polymeric patterns pose additional challenges as they often degrade in the electron beam. Nondestructive, high-resolution shape measurements are critical to fully optimize NIL processes.

Specular x-ray reflectivity (SXR) is a high precision technique for measuring the thickness, density, and roughness of thin, blanket films.[6] In this letter SXR is extended from smooth to patterned surfaces, where the patterns are sub μm in range. For smooth films, the layer thickness, free-surface roughness, interfacial roughness between the layers, and the density profile as a function of distance perpendicular to the film surface are deduced by modeling the x-ray reflectivity with a one-dimensional Schrödinger equation.[6,7] This modeling is applied to patterned surfaces to quantify the pattern height, residual layer thickness, and the line-to-space ratio. If the pitch or linewidth is known, the relative linewidth variations can be converted into absolute length scales to fully quantify the line shape profile.

An imprint master of parallel lines and spaces patterned into the silicon oxide (SiO_x) surface of a 10.16 cm (4 in.) diameter silicon wafer was purchased from Nanonex.[8] Critical dimension small angle x-ray scattering (CD-SAXS)[9,10] measurements of the patterns indicate a pitch of (1945 ± 5)[11] Å and nominally a trapezoidal line cross section with an average linewidth of (772 ± 10) Å, an average line height of (1650 ± 50) Å and slightly asymmetric sidewall angles of $\beta_{\text{left}}=(5.4\pm0.5)^\circ$ and $\beta_{\text{right}}=(6.3\pm0.5)^\circ$. The patterns were thermally imprinted from the mold into a NXR-1020 resist on a NX-2000 imprint tool, both from Nanonex. The SXR measurements were performed on a reflectometer that is specified elsewhere in detail.[12] The X rays have wavelength $\lambda=1.54$ Å and are incident onto the sample at a grazing angle θ. A detector is situated at an equal exit angle θ and the intensity is measured as a function of $Q=4\pi/\lambda\sin(\theta)$. The mold and the imprinted pattern were always mounted with the line orientation perpendicular to the plane defined by the surface normal and the incident beam. Although we do not show the data here, the parallel orientation yielded nearly identical results.

The logarithm of the reflectivity ratio, $\log(R)$, is plotted as a function of Q for both the mold and the imprinted pattern in Fig. 1. Also shown are the theoretical reflectivity curves for both a smooth silicon surface and infinitely thick resist films. The Kiessig fringes in the experimental data from the mold indicate a supported film with an appreciable density difference between the film and the substrate. This data are striking because the mold is a *single* material of uniform density. The suggestion of two densities is supported by the observation of two critical angles, one near $Q_{c,\text{Si}}=0.0322$ Å^{-1} and another at $Q<Q_{c,\text{Si}}$. The square of Q_c is proportional to the electron density ρ_e through the expression $Q_c^2=16\pi r_o\rho_e$, where r_o is the classical electron radius. The coincidence of $Q_{c,\text{Si}}$ with Q_{c,SiO_x} is reasonable given that the electron densities of Si and SiO_x can be nearly identical. However, a material significantly less dense than Si or SiO_x, as suggested by the experimental data for the mold, is not possible. A plausible explanation for the lowest critical angle is illustrated in the upper schematic of Fig. 2(a). The density across the topology of the pattern is averaged by SXR, giving the signature of a homogeneous layer of lower density. The planar layer equivalent model shown to the right of the mold cartoon in Fig. 2(a) is fit to the data in Fig. 1 (solid line) with excellent agreement. Likewise, the imprinted

[a]Author to whom all correspondence should be addressed; electronic mail: csoles@nist.gov

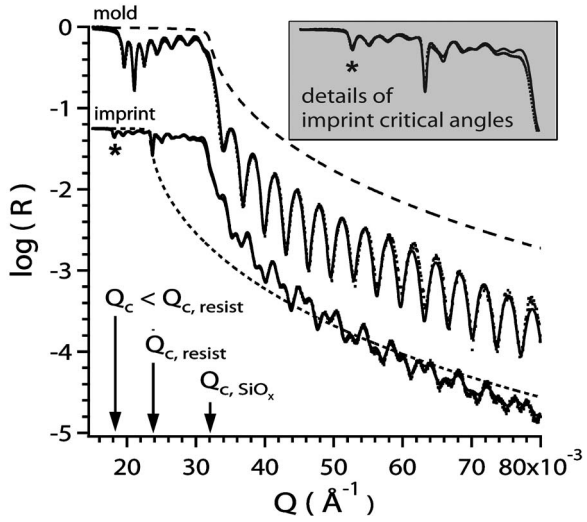

FIG. 1. The experimental reflectivity is shown for the mold (upper curve) and the imprinted pattern (lower curve, vertically offset). The solid lines through the data points indicate the model fits described in the text. The long and short dashed lines are theoretical reflectivity curves for a smooth, infinitely thick Si and resist surface, respectively. The inset magnifies the reflectivity for the imprinted sample in the region of the asterisk near the three critical angles.

sample consists of discrete resist patterns over a residual layer of the same resist material, all supported on a Si wafer. In Fig. 1, the two critical angles of Si and the resist ($Q_{c,\mathrm{resist}}=0.0233$ Å^{-1}) are complemented by a third at $Q < Q_{c,\mathrm{resist}}$. Consistent with the mold interpretation, the reflectivity is fit (solid line, Fig. 1) to the equivalent bilayer model on a SiO_x substrate depicted in Fig. 2(a), where the intermediate layer is the residual layer of resist and the top layer has a density less than the resist.

The fits from Fig. 1 are presented in Fig. 3 in terms of the scattering length density Q_c^2 as a function of distance z. $Q_c^2 \propto \rho_e \propto \rho_{\mathrm{mass}}$, thereby establishing the physical density profiles through the films. For the resist, $Q_c^2=0$ at the free surface or top of the pattern and increases to approximately 0.35×10^{-3} Å^{-2} for the next 1720 Å before increasing to the pure resist value of 0.542×10^{-3} Å^{-2}. Q_c^2 remains constant for the next 1281 Å before increasing abruptly to 0.104×10^{-2} Å^{-2} at the resist/SiO_x interface. The direct interpretation is that the average pattern height is (1720±10) Å and the average residual layer thickness is (1281±10) Å. Figure 2(b) demonstrates that these values are nominally consistent with the scanning electron microscopy (SEM) cross section of the imprinted pattern. However, the level of confidence in the dimension extracted from the SEM images is limited. The Nanonex 1020 resist was very sensitive to electron beam degradation; the sample dimension would decay while the image was collected. To reduce this damage, the image in Fig. 2(b) was obtained at a low accelerating voltage (0.5 keV) and beam current (2.5 μA). A conductive gold or metal coating was not applied because their thickness becomes significant compared to the size of the features of interest.

A similar interpretation is made for the mold profile in Fig. 3. Starting from $z=0$ Å at the SiO_x substrate for the mold, Q_c^2 decreases rapidly from a value consistent with pure Si (0.104×10^{-2} Å^{-2}) to approximately 0.4×10^{-3} Å^{-2} farther away from the substrate. This value changes slightly with z for the next 1731 Å, at which point Q_c^2 drops to zero. This means that the cavity depth or pattern height in the

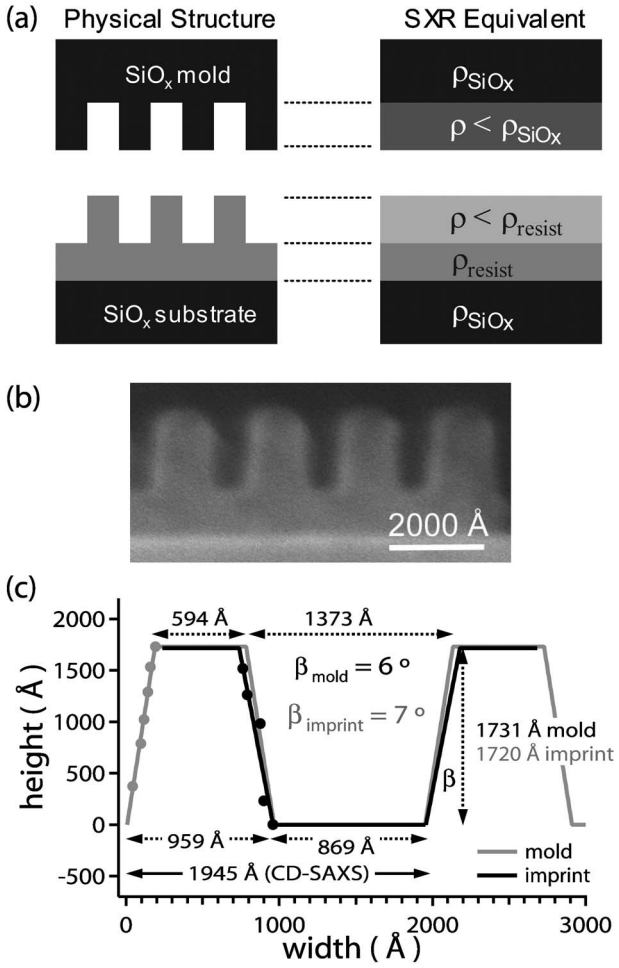

FIG. 2. The cartoons on the left hand side of part (a) depict the structures of the mold and the imprinted pattern while the cartoon to the right indicates the equivalent layer model used to model the SXR data. The image in part (b) is a SEM cross section of the actual imprinted structure, indicating the line height and residual layer thickness from the SXR analysis are reasonable. Part (c) quantifies the line shape profiles for the mold and the imprint and shows how well the features in the imprint replicate the mold.

mold is (1731±10) Å. The CD-SAXS pattern height of the mold is (1650±50) Å, just beyond the state range of the SXR uncertainty. This slight disagreement may result from the model used to interpret the CD-SAXS data. A simple trapezoidal cross section was assumed, but the density profiles in Fig. 3 suggest that the top and bottom corners of the features are more gently rounded.

The line-to-space ratio can be determined by comparing Q_c^2 in the patterned region to the fully dense material. This is illustrated in Fig. 3 with the line marked "l" and "s" for line and space, respectively. The Q_c^2 of the pure resist is 0.542×10^{-3} Å^{-2} while the patterned region displays an average of $Q_c^2 \approx 0.35\times10^{-3}$ Å^{-2}. The fraction of area filled in the patterned region is then approximately $0.35/0.542=0.65$, i.e., a line-to-space ratio of 1.4. This line-to-space ratio is consistent with the value of 1.5 measured by CD-SAXS and the SEM cross-section image in Fig. 2(b). The line-to-space ratio cannot be transformed into a physical linewidth from the SXR data alone. An external length scale is needed, such as the measured CD-SAXS pitch of (1945±5) Å. From the Q_c^2 profiles and the CD-SAXS pitch, the complete line shape profiles are quantified for both the mold and the imprinted pattern. These profiles are overlaid in Fig. 2(c) to illustrate

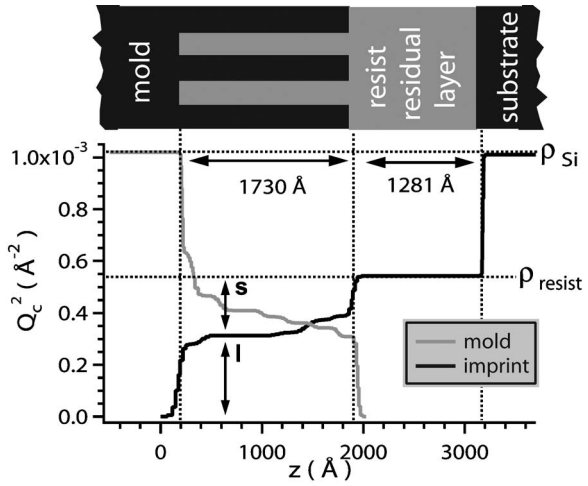

FIG. 3. The scattering length density (Q_c^2) profile is shown as a function of distance z through the structures. The cartoon at the top of the figure (the linewidths are not drawn as trapezoids and are not to scale) correlates which regions of the mold or imprint structure correspond to which regions of the scattering length density profile.

how well the cavities in the mold match the features in the imprint. One caveat is that this conversion provides an *average* line shape profile and does not distinguish between left and right sides of the pattern. For clarity the experimental profile data points for the mold are shown on just the left side of one line (gray circles) while the mold points are shown on the right (black circles). Linear fits through these experimental points estimate average sidewall angles of $\beta_{\text{mold}}=6°$ and $\beta_{\text{imprint}}=7°$. These are consistent with the CD-SAXS measurements of $\beta_{\text{left}}=(5.4\pm0.5)°$ and $\beta_{\text{right}}=(6.3\pm0.5)°$ for the mold. To within experimental error, the pattern widths, heights, and sidewall angles are consistent between the mold and imprint. This indicates an excellent fidelity of pattern transfer from the mold to the imprint.

The measurements described herein do not require specialized equipment and can be performed on a commercial x-ray diffractometer setup to perform reflectivity. Data collection times are approximately 1 h per sample, although faster measurements would be possible with a more powerful rotating anode source or a synchrotron. The footprint of the beam on the sample at grazing angles is large, on the order of few cm^2, so large area samples are required. Microfocus x-ray sources will help reduce this footprint to a few mm^2 and facilitate local measurements. Increasing λ can also push Q_c to higher angles, further decreasing the footprint. It should also be realized that SXR provides average dimensions, averaged over many structures. This should be considered when interpreting the average value of the length scale or dimension being quantified. If the structures are dissimilar in terms of their residual layer thickness, height, widths, or aperiodic, the utility in knowing the average becomes less useful for reconstructing the shape of the features. Finally, while the current analysis applies to patterns of nm scale, larger scale structures may require additional consideration of the x-ray coherence length.[13,14]

In summary, SXR can be used to quantify pattern height, residual layer thickness, and the line-to-space ratio for patterns on the order of 100 nm. If the pitch, pattern width, or some other lateral length scale is known, the line-to-space ratio can be converted into absolute linewidths. This can be used to calculate the line shape profile in both the mold and imprinted patterns, enabling high precision fidelity of pattern transfer studies.

The authors acknowledge the NIST Office of Microelectronics and the ATP Intramural Funding Program for financial support and the Nanonex Corporation for their assistance in fabricating the imprint patterns.

[1]S. Y. Chou, P. R. Krauss, and P. J. Renstrom, Science **85**, 272 (1996); S. Y. Chou, P. R. Krauss, W. Zhang, L. Guo, and L. Zhuang, J. Vac. Sci. Technol. B **15**, 2897 (1997).
[2]M. D. Austin, H. He, W. Wu, M. Li, Z. Yu, D. Wasserman, S. A. Lyon, and S. Y. Chou, Appl. Phys. Lett. **84**, 5299 (2004).
[3]C. Gourgon, C. Peret, G. Micouin, F. Lazzarino, J. H. Tortai, O. Jorbert, and J.-P. E. Grolier, J. Vac. Sci. Technol. B **21**, 98 (2003).
[4]H. Schulz, M. Wissen, and H.-C. Scheer, Microelectron. Eng. **67, 68**, 657 (2003).
[5]C. Perret, C. Gourgon, G. Micouin, and J.-P. Grolier, Jpn. J. Appl. Phys., Part 1 **41**, 4203 (2002).
[6]L. G. Parrat, Phys. Rev. **95**, 359 (1954).
[7]J. F. Ankner, and C. J. Majkrzak, Proc. SPIE **1738**, 260 (1992).
[8]Certain commercial materials and equipment are identified in this letter in order to specify adequately the experimental procedure. In no case does such identification imply recommendation by the National Institute of Standards and Technology nor does it imply that the material or equipment identified is necessarily the best available for this purpose.
[9]R. L. Jones, T. J. Hu, E. K. Lin, W.-L. Wu, R. K. Kolb, D. M. Casa, P. Boulton, and G. G. Barclay, Appl. Phys. Lett. **83**, 4059 (2003).
[10]T. J. Hu, R. L. Jones, E. K. Lin, W.-L. Wu, D. Keane, S. Weigand, and J. P. Quintana, J. Appl. Phys. **96**, 1983 (2005).
[11]The uncertainties in all of the dimensional quantities presented in the letter are estimated quantities. The standard uncertainty from the χ^2 of the fit is always less than this estimated uncertainty, but meaningless because user selected variations of the physical model have more influence on fitted values.
[12]H.-J. Lee, C. L. Soles, D.-W. Liu, B. J. Bauer, and W.-l. Wu, J. Polym. Sci., Part B: Polym. Phys. **40**, 2170 (2002).
[13]T. P. Russell, in *Materials Science Reports* (Elsevier, North–Holland, Amsterdam, 1990), Vol. 5, p. 171.
[14]M. Tolan, W. Press, F. Brinkop, and J. P. Kotthaus, Phys. Rev. B **51**, 2239 (1995).